Advanced Robotics

ISSN: 0169-1864 (Print) 1568-5535 (Online) Journal homepage: https://www.tandfonline.com/loi/tadr20

Workspace evaluation of Stewart platforms

Oren Masory & Jian Wang

To cite this article: Oren Masory & Jian Wang (1994) Workspace evaluation of Stewart platforms, Advanced Robotics, 9:4, 443-461, DOI: 10.1163/156855395X00508

To link to this article: https://doi.org/10.1163/156855395X00508

Published online: 02 Apr 2012.

Submit your article to this journal

Article views: 170

View related articles

Citing articles: 11 View citing articles

Full Terms & Conditions of access and use can be found at
https://www.tandfonline.com/action/journalInformation?journalCode=tadr20

Advanced Robotics, Vol. 9, No. 4, pp. 443–461 (1995)
© VSP and Robotics Society of Japan 1995.

Regular Papers

Workspace evaluation of Stewart platforms

OREN MASORY and JIAN WANG
Robotics Center, Florida Atlantic University, Boca Raton, FL 33431, USA

Received for *AR* 21 February 1992; accepted 23 June 1993

Abstract—The workspace and the dexterity of a Stewart platform are affected by the choice of its major dimensions, actuator stroke and the kinematic constraints of its joints. An investigation of the effects of these parameters on workspace volume of the platform is presented. The obtained results were normalized so that they could be used as a design tool for the selection of dimensions, joints and actuators.

1. INTRODUCTION

Most industrial robots are open-chain mechanisms which are constructed of consecutive links connected by rotational or prismatic 1 d.o.f. joints. These serial manipulators have a large workspace, high dexterity and maneuverability. However, due to their serial structure they exhibit low stiffness and poor positioning accuracy. As a result, their use in applications that require large loads (e.g. machining) and high accuracy is limited. Therefore, in recent years, effort and attention have been given to parallel manipulators. In a parallel manipulator, the end effector is attached to a moveable plate which is supported in-parallel by a number of actuated links. It has been recognized that this kind of manipulator possesses the following advantages compared with serial manipulators: (i) high accuracy due to the non-cumulative joint errors, (ii) high force/torque capacity since the load is distributed to several in-parallel actuators and (iii) high structural rigidity. Therefore, these are suitable for applications in which high speed, high positioning accuracy and fast dynamic response are required. However, despite these advantages, these manipulators do have a major drawback, i.e. their restricted workspace.

The first parallel actuated mechanism was originally proposed by D. Stewart as an aircraft simulator [1], hence the so-called 'Stewart platform'. Once the drawbacks of serial manipulators were recognized, parallel manipulators attracted considerable attention. Topics including inverse and forward kinematics analysis [2–6], dynamics [7, 8], workspace analysis [9–12], practical design/construction considerations [2], calibration [13], and a variety of applications [14–23] have been addressed in literature.

The workspace of a Stewart platform can be defined as a reachable region of the origin of a coordinate system attached to the center of the moving plate. Since its

major drawback is a restricted workspace, it is of primary importance to develop algorithms by which the workspace can be determined and the effect of different designs on the workspace can be evaluated. Determination of a parallel manipulator workspace is rather difficult, compared with serial manipulators, due to: (i) an analytic solution of its forward kinematic problem, which involves the solution of a set of highly non-linear simultaneous equations, is not available; and (ii) the workspace also depends on constraints introduced by joint angle limitations, link length limitations and interference between the links. Few published reports are concerned with this issue. In [9] the workspace of a special case platform, where all joints are evenly distributed and the payload platform is allowed to rotate only about one axis, was analyzed. In [10] the workspace of a 3 d.o.f. parallel manipulator was simulated. Algorithms for the determination of the workspace of a Stewart platform, based on numerical discretization of Cartesian space and integration of all workspace blocks, were proposed in [11, 12]. In [25, 26] the effect of link length and link interference on the workspace of a particular platform was investigated. However, in all other references physical constraints such as joint angle limitations, link interference and geometric parameters, which exist in practical system, were not considered.

Since in many cases the manipulator workspace determines its applicability for the task, optimizing the workspace of parallel manipulators is essential in order to expand their range of applications. The purpose of this study is to present the effects of all kinematic constraints on the Stewart platform workspace. This information can be used by a designer to determine dimensions and specify the joint range of rotation, so that the maximum workspace can be obtained.

This paper is organized as follows. First, geometric parameters and kinematic constraints related to the workspace of the Stewart platform are described and a kinematic model for workspace evaluation is established. Secondly, a computer algorithm is presented to calculate the workspace of a Stewart platform, where all the constraints are taken into account. Third, based on a proposed workspace criterion, the effects of different manipulator geometric parameters and constraints on the workspace are investigated. The parameters and constraints include joint locations on the plate and the base, radius ratio of two plates, joint angle limitations, link length limitations and link interference.

2. GEOMETRIC PARAMETERS AND KINEMATIC CONSTRAINTS

2.1. Coordinate system and geometric parameters

The Stewart platform, illustrated in Fig. 1, is composed of six variable length links, a fixed base and a movable plate to which the tool is attached. It is assumed that the base and the plate are circular with radii R_b and R_p, respectively. A base coordinate system $\{B\}$ is placed at the base center O_b with its Z-axis perpendicular to the base plane. Similarly, the coordinate system $\{P\}$ is located at the center of the moving

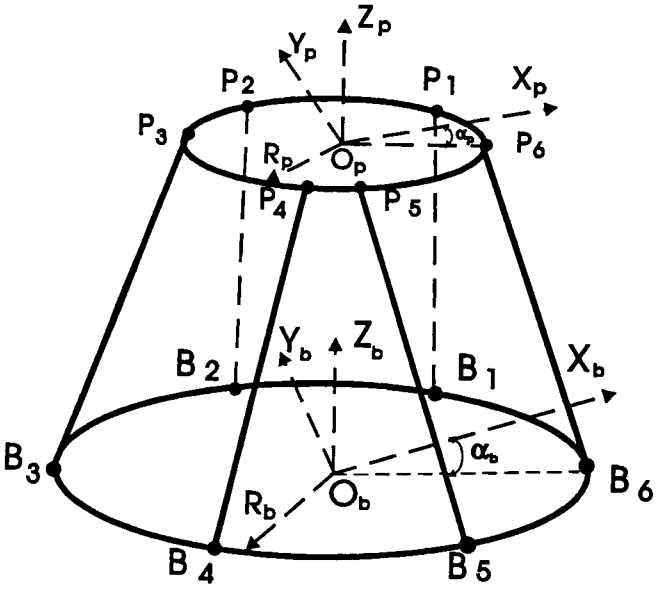

Figure 1. Stewart platform parameters' definitions.

plate. The joints pairs attached to the plate and the base are denoted by P_1 to P_6 and B_1 to B_6, respectively.

The coordinates of B_i, $i = 1, \ldots, 6$, with respect to $\{B\}$ are denoted as b_i, and those of P_i with respect to $\{P\}$ as p_i. The X-axis of $\{B\}$ is selected along the line which bisects the angle $B_1 O_b B_6$, and similarly for the X-axis of $\{P\}$. Denote half of the angle $B_1 O_b B_6$ as the base angle, α_b, and half of the angle $P_1 O_p P_6$ as the plate angle, α_p. These angles are used to define the location of joints on the base and the plate relative to $\{B\}$ and $\{P\}$, respectively:

$$\begin{aligned} b_i &= R_b(\cos\alpha_{b_i}, \sin\alpha_{b_i}, 0) \\ p_i &= R_p(\cos\alpha_{p_i}, \sin\alpha_{p_i}, 0) \end{aligned} \tag{1}$$

where $i = 1, \ldots, 6$, and

$$\begin{aligned} \alpha_{b_1} &= \alpha_b & \alpha_{p_1} &= \alpha_p \\ \alpha_{b_2} &= 120^\circ - \alpha_b & \alpha_{p_2} &= 120^\circ - \alpha_p \\ \alpha_{b_3} &= 120^\circ + \alpha_b & \alpha_{p_3} &= 120^\circ + \alpha_p \\ \alpha_{b_4} &= 240^\circ - \alpha_b & \alpha_{p_4} &= 240^\circ - \alpha_p \\ \alpha_{b_5} &= 240^\circ + \alpha_b & \alpha_{p_5} &= 240^\circ + \alpha_p \\ \alpha_{b_6} &= 360^\circ - \alpha_b & \alpha_{p_6} &= 360^\circ - \alpha_p \end{aligned}$$

2.2. *Kinematic constraints*

Three types of kinematic constraints affect the available workspace of a Stewart platform: link length limitations, joint angle limitations and link interference.

2.3. Link length limitations

The plate pose can be described by a 3×3 orientation matrix R and a translation vector q which define $\{P\}$ with respect to $\{B\}$. l_i, the vectors connecting B_i to P_i expressed in $\{B\}$, where $i = 1, 2, \ldots, 6$ indicates the leg number, are given by:

$$l_i = Rp_i + q - b_i \tag{2}$$

The links length, denoted as L_1 to L_6, are given by:

$$L_i = |Rp_i + q - b_i| \tag{3}$$

The link length constraint is expressed by:

$$L_{\min_i} \leqslant L_i \leqslant L_{\max_i} \tag{4}$$

where $L_{\min_i}$ and $L_{\max_i}$ are the minimum and maximum allowable length of link i.

2.4. Joint angle constraints

The links are typically attached to the plate by ball joints and to the base by U-joints. A ball joint is free to rotate about all three axes; however, in practice, its motion is restricted by the physical construction of the joint. As shown in Fig. 2, the rotational angle of a ball joint, θ, defined as the angle between the Z-axis of a coordinate system attached to its socket, and u, a vector along the leg connected to the joint, is

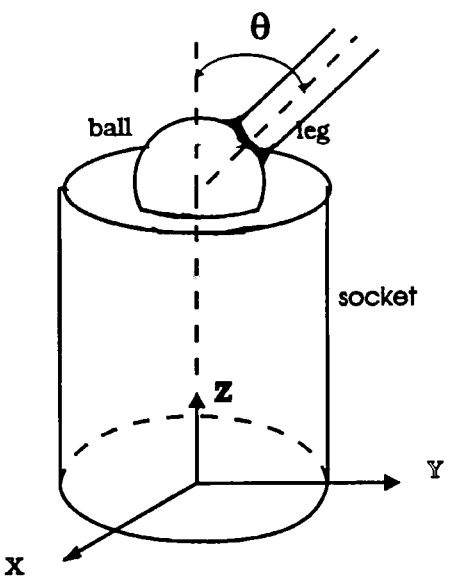

Figure 2. Ball joint rotational angle definition.

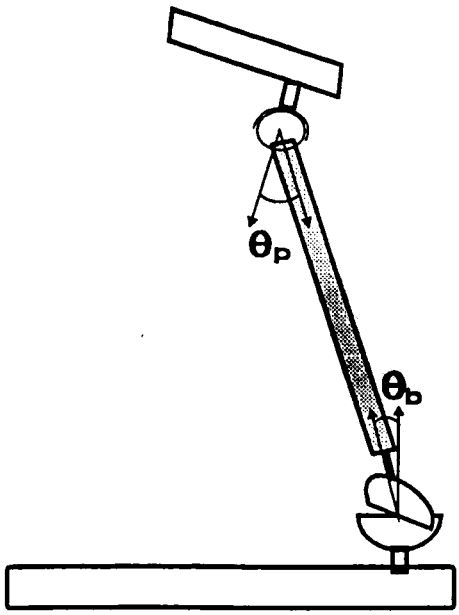

Figure 3. Joint rotational constraints.

physically constrained. The rotation angle of a U-joint is restricted in a similar way. In other words, every practical joint has its maximum rotational angle $\theta_{\max}$.

Assume that the socket of a ball joint i is installed so that a unit vector n_{p_i} describes its orientation with respect to $\{P\}$. The rotational angle of a ball joint and its constraint can be computed by:

$$\theta_{p_i} = \cos^{-1} \frac{l_i \cdot Rn_{p_i}}{|l_i|} \leqslant \theta_{p_{max}} \tag{5a}$$

Similarly, for an isotropic U-joint the rotational angle is given by (see Fig. 3):

$$\theta_{b_i} = \cos^{-1} \frac{l_i \cdot n_b}{|l_i|} \leqslant \theta_{b_{max}} \tag{5b}$$

where n_{b_i} is the unit vector which describes the U-joint orientation with respect to $\{B\}$, and $\theta_{b_{max}}$ and $\theta_{p_{max}}$ are the maximum allowable rotational angles of the ball and the U-joints, respectively.

The joints can also be installed along a particular direction. If each joint is installed along its nominal direction l_{n_i}, which is the direction of vector l_i when each link length is equal to $0.5(L_{\min_i} + L_{\max_i})$ and the plate has no rotation with respect to the base, then the rotational angles are given by:

$$\theta_{p_i} = \cos^{-1} \frac{l_i \cdot Rl_{n_i}}{|l_i|\,|l_{n_i}|} \tag{6a}$$

and

$$\theta_{b_i} = \cos^{-1} \frac{l_i \cdot l_{n_i}}{|l_i|\,|l_{n_i}|} \tag{6b}$$

With such installation, it is possible to substantially increase the platform workspace, as will be shown in the simulation results below.

2.5. *Link interference constraints*

Since links have physical dimensions, interference might occur. For the sake of analysis assume that each link is cylindrical with a diameter D. Let D_i $(i = 1, \ldots, 6)$ be the shortest distance between the center lines of two adjacent links, the interference constraint can be expressed by:

$$D_i \geqslant D \tag{7}$$

Let n_i be a unit vector in the direction of the common normal between two consecutive link vectors l_i and l_{i+1}:

$$n_i = \frac{l_i \times l_{i+1}}{|l_i \times l_{i+1}|} \tag{8}$$

Δ_i, the shortest distance between the two lines defined by the vectors l_i and l_{i+1}, as shown in Fig. 4, is given by:

$$\Delta_i = \left|n_i \cdot (b_{i+1} - b_i)\right| \tag{9}$$

It should be stressed that in general the shortest distance between links (D_i) is not necessarily equal to the shortest distance between the link vectors (Δ_i). The relationship between the two depends on the location of the intersection points (C_i and C_{i+1}) of the link vectors l_i, l_{i+1} with their common normal n_i. The coordinates c_i of C_i can be computed by (see Appendix A for derivation):

$$\frac{c_i - b_i}{{}^{B}p_i - b_i} = \left|\frac{(b_{i+1} - b_i) \cdot m_i}{({}^{B}p_i - b_i) \cdot m_i}\right| \tag{10}$$

where ${}^{B}p_i$ are the coordinates of P_i with respect to $\{B\}$ and m_i is a vector defined by:

$$m_i = n_i \times ({}^{B}p_{i+1} - b_{i+1}) \tag{11}$$

Similarly for c_{i+1}. According to the location of C_i and C_{i+1}, three different cases need to be distinguished:

Case 1: Both intersection points are on the links

In this case, as shown in Fig. 4(a), $D_i = \Delta_i$, and interference occurs if $D_i > \Delta_i$.

Case 2: One of the intersection points is outside the link.

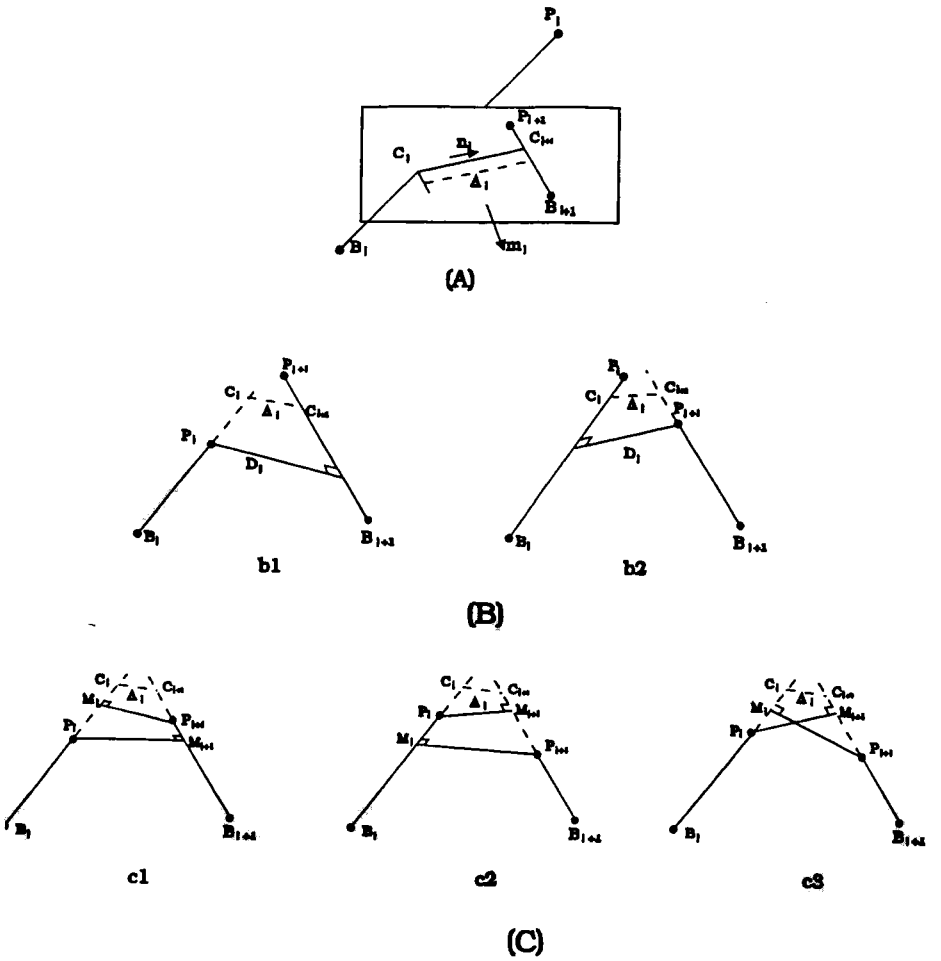

Figure 4. Different cases of link interference.

In this case, as shown in Fig. 4(b), the distance D_i can be determined according to the positions of the two intersection points. As shown in Fig. 4(b1), if C_i is located beyond P_i, but C_{i+1} is on the $(i+1)$th link, then D_i, which is the distance from P_i to the $(i+1)$th link, is given by:

$$D_i = \frac{\left|\left({}^{\mathrm{B}}p_i - b_{i+1}\right) \times l_{i+1}\right|}{|l_{i+1}|} \tag{12}$$

if C_{i+1} is located beyond P_{i+1}, but C_i is on the ith link as shown in Fig. 4(b2), then D_i, which is the distance from P_{i+1} to the ith link, is given by:

$$D_i = \frac{\left|\left({}^{\mathrm{B}}p_{i+1} - b_i\right) \times l_i\right|}{|l_i|} \tag{13}$$

Case 3: Both intersection points are not on the links

In this case, as shown in Fig. 4(c), D_i depends on the location of M_i, which is the intersection point between l_{i+1} and the normal from point P_i to vector l_{i+1}, and the location of M_{i+1}, which is the intersection point between l_i and the normal from P_{i+1} to vector l_i. There are three possibilities:

(1) If M_{i+1} is located on the link $P_{i+1}B_{i+1}$ while M_i is out of the link P_iB_i, as shown in Fig. 4(c1), then D_i is given by equation (12).

(2) If M_i is located on the link P_iB_i while M_{i+1} is out of the link $P_{i+1}B_{i+1}$, as shown in Fig. 4(c2), then D_i is given by equation (13).

(3) If both M_i and M_{i+1} are located out of the links, as shown in Fig. 4(c3), then D_i is the distance between two joints P_i and P_{i+1}.

3. WORKSPACE CRITERION AND DETERMINATION

The workspace of the Stewart platform can be defined as the three-dimensional Cartesian space which is reachable by the center of the moving plate, i.e. the origin of $\{P\}$. Since the workspace of a Stewart platform is closed, the volume of the workspace can be used as a criterion for workspace evaluation and optimization. Furthermore, the volume of the workspace for different platform orientations can be used as a measure of the platform dexterity. The workspace volume is a function of the geometric parameters as well as the kinematic constraints of the platform. Therefore, the volume criterion can also be used to evaluate the effect of different geometric parameters and kinematic constraints on the workspace.

For every pose (position and orientation) of $\{P\}$ the links length L_i, joint rotational angle θ_{p_i}, θ_{b_i} and the distance between link pairs, D_i, can be determined as described in the previous sections. These values are then compared with a given set of physical constraints L_{max}, L_{min}, $\theta_{p_{max}}$, $\theta_{b_{max}}$ and D. If any of the constraints is violated, the particular pose is not reachable and therefore is out of the workspace. Similarly, if all of the constraints are satisfied, the pose is reachable and is within the workspace.

The workspace volume, V, was computed as follows:

(1) The workspace was divided into slices of thickness ΔZ parallel to the $X-Y$ plane, as shown in Fig. 5.

(2) The boundaries of each slice were found and the volume of each slice was calculated.

(3) The volume of the platform workspace is computed by summing all slice volumes.

A program that calculates the workspace volume according to the above procedure was written. In this regard, a few points should be emphasized:

(1) The search for a pose, which is within the workspace, starts at the plane $Z = Z_0$ which lies well below (does not intersect) the workspace. Note that Z_0 is not necessarily defined by the plane where all links are at minimum length ($L_i = L_{min}$) and therefore Z_0 should be less than Z_{min}.

(2) The search ends at the plane Z_{max} which contains only one feasible pose.

(3) The intersection of the workspace with a plane parallel to the $X-Y$ plane is in most cases a simply-connected domain. In this case, the boundary of the slice is found using a fast search method illustrated in Fig. 6. Assume that a point A_1 on the boundary was obtained by increasing radius ρ until one constraint is violated. Then the angle γ is increased by $\Delta\gamma$ and the coordinates of the point T_1 are calculated using the values $\gamma_i + \Delta\gamma$ and ρ_i. If the point is within the workspace, ρ is increased gradually until a constraint is violated and a new boundary point (A_2 in Fig. 6) is found. Otherwise, if the new point is out of the workspace (T_2 in Fig. 6), ρ is decreased gradually until a new boundary point is found (A_3 in Fig. 6). Once all boundary points are registered, the volume of the slice is determined by:

$$V_i = \frac{1}{2}\sum_j \rho_j^2 \Delta\gamma \Delta Z \tag{14}$$

(4) In some cases, as shown in Fig. 7, the intersection is not a simply-connected domain, which often happens in the lower part of the platform workspace. In Fig. 7, the hatched area is within the workspace. Therefore, the search radius ρ_{max} should be large enough to cover the whole region. In this case the volume of the slice is given by:

$$V_i = \frac{1}{2}\sum_j (\rho_{j_1}^2 + \rho_{j_2}^2 - \rho_{j_3}^2)\Delta\gamma \Delta Z \tag{15}$$

The workspace volume, V, is computed by summing up the volumes of all slices.

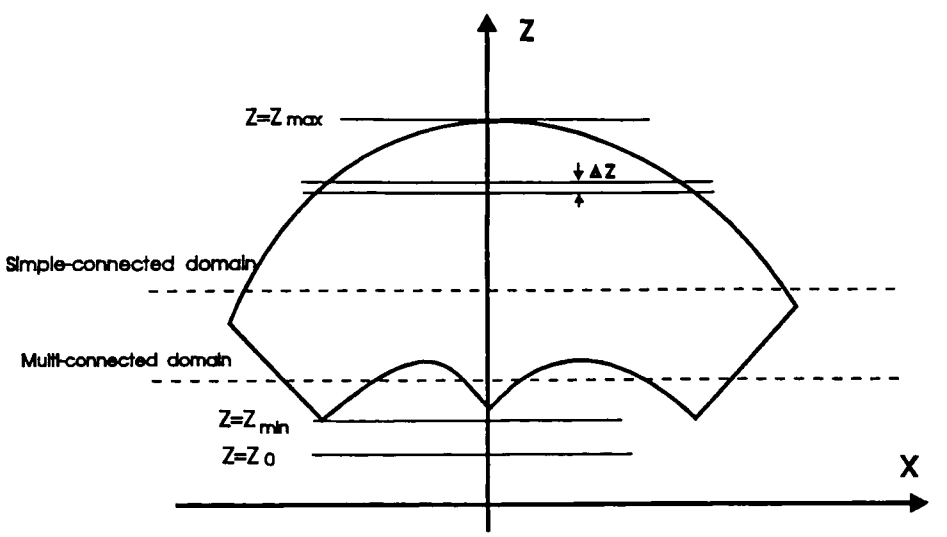

Figure 5. Definitions for workspace slicing in the vertical direction.

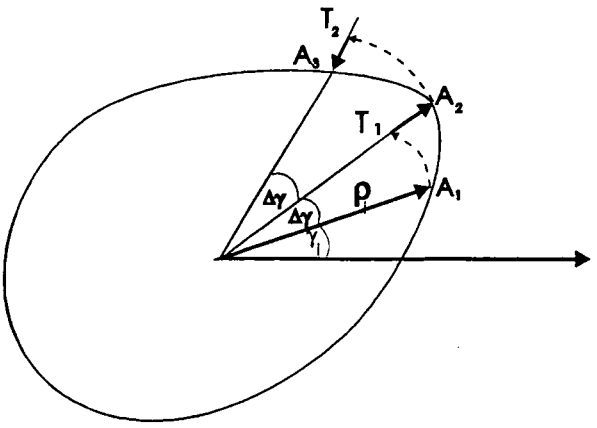

Figure 6. Searching method for workspace boundaries.

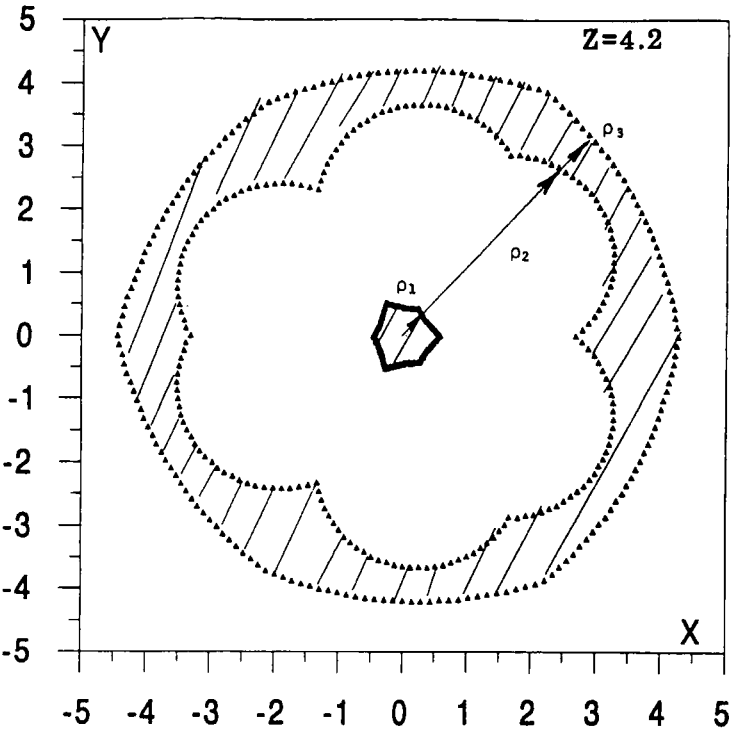

Figure 7. An example of multi-connected domain.

4. EFFECTS OF DIFFERENT PARAMETERS AND CONSTRAINTS

The effects of different geometric parameters and kinematic constraints on the workspace and dexterity of a Stewart platform are presented in this section. The results were obtained by changing a particular parameter of a platform while keeping all others constant.

4.1. Workspace of a 'normalized platform'

A 'normalized platform', in which all dimensions are normalized with respect to R_p, was used in this study. Its dimensions, joint locations and kinematic constraints are defined by:

$$R_p = 1 \qquad R_b = 3 \qquad \alpha_p = 15^\circ \qquad \alpha_b = 30^\circ$$

$$\theta_{pmax} = \theta_{bmax} = 45^\circ$$

$$L_{min} = 4.5 \qquad L_{max} = 7.5$$

$$D = 0.1$$

A Stewart platform, with the above parameters and constraints, was simulated and the resulting workspace is demonstrated by cross-sections along the Y- and Z-axes as shown in Fig. 8. Three cases are considered:

(1) The plate orientation, defined by roll, pitch and yaw angles, was constrained to move parallel to its base (roll = pitch = yaw = 0) (shown in Fig. 8a and b).

(2) The roll, pitch and yaw angles were changed from 0° to +5°, +10° and +15° simultaneously (shown in Fig. 8c and d).

(3) The roll, pitch and yaw angles were varied from 0° to +10° and from 0° to −10°, (shown in Fig. 8e and f).

Observing these figures the following conclusion can be drawn:

(1) The surface that contains the workspace is composed of three sections determined by three constraints: (a) upper dome constrained by L_{ax}, (b) conical surface constrained by the joint angle limitations and (c) bottom dome constrained by L_{min} (Fig. 8a and b).

(2) For roll = pitch = yaw = 0°, the platform workspace is symmetrical about the Z-axis while for any other orientation it is not.

(3) The workspace of the platform is substantially decreased as the orientation requirements increase (Fig. 8c–f).

4.2. Effect of kinematic constraints

4.2.1. Joint angle constraint. The workspace volume, V, for different end-effector orientations versus joint angle limitations (all other parameters and constraints are nominal) is illustrated in Fig. 9 (RPY are the roll, pitch and yaw angles of the plate). As shown, this constraint has a significant effect on the workspace volume and for large orientation angles the volume can be zero, which means that the platform is locked. The effect of the joint angle is further demonstrated in Fig. 10.

Although the maximum rotational angle of the joints cannot be changed once the joints have been selected, it is possible to enlarge the workspace by fully utilizing their range of rotation. Rather than mounting the joints perpendicular to the base and the plate plane, it is advantageous to install them along the direction of the vector l_{n_i}. Comparing the results shown in Fig. 11 to the ones in Fig. 9, the workspace volume in this case is increased about three times for joints with limited rotational angle. This improvement is clearly shown in Fig. 12 when compared with Fig. 8.

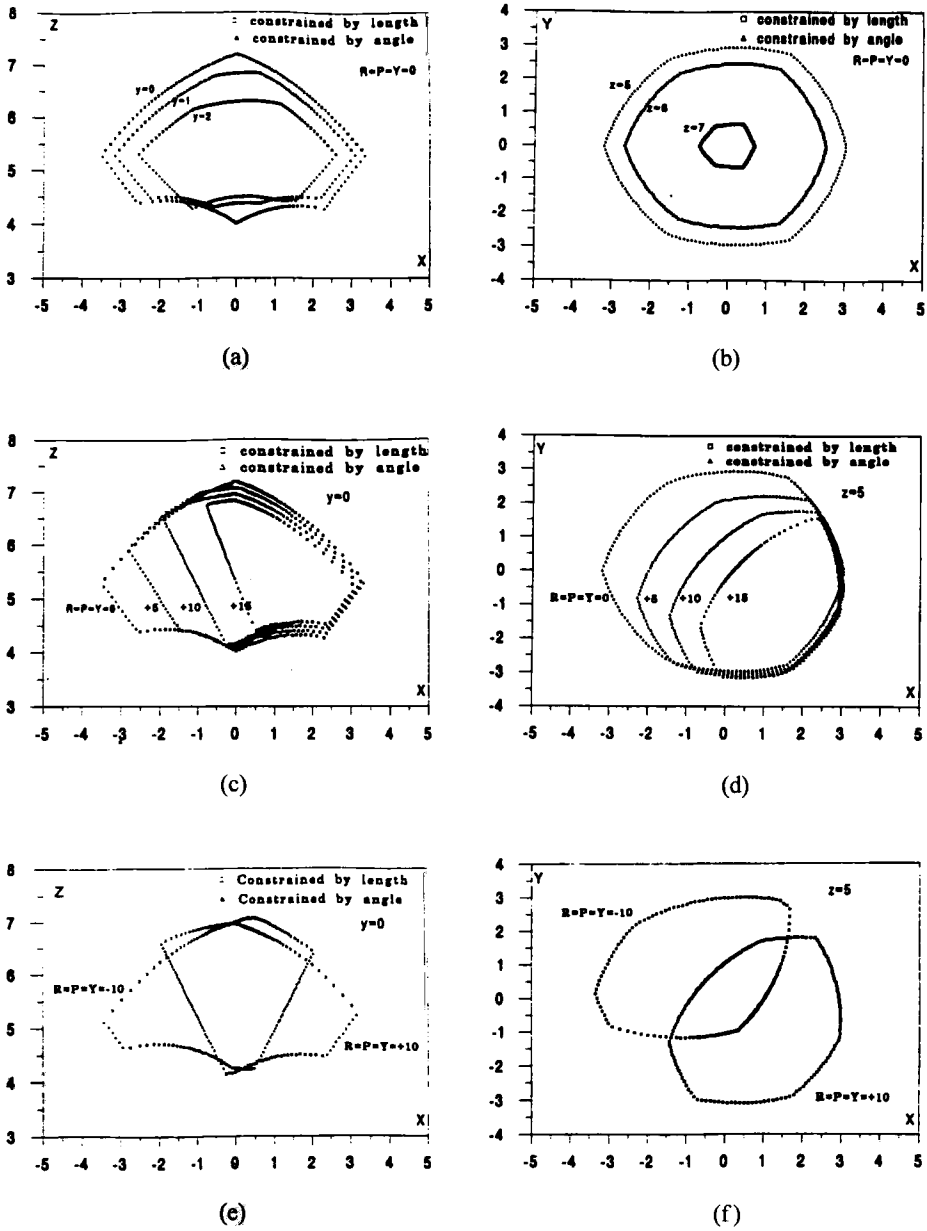

Figure 8. Workspace of the 'Normalized Platform'.

4.2.2. Link length constraint. In practice, $L_{\min}$ can be approximated by the travel range of the link, S, plus a constant, C (in thus case of a hydraulic actuator this corresponds to the actuator's stroke plus a constant). Thus, $L_{\min}$ and $L_{\max}$ can be expressed by:

$$L_{\min} = S + C \tag{16}$$

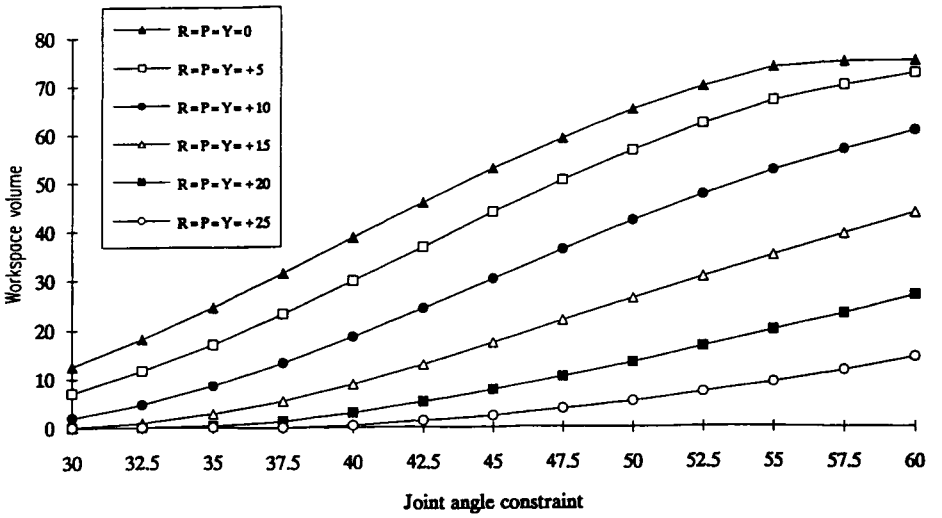

Figure 9. Workspace volume versus joint angle constraints.

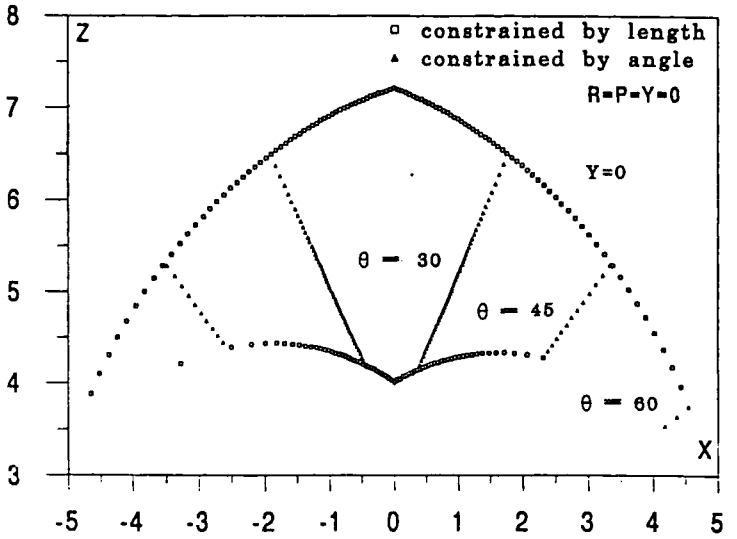

Figure 10. Workspace boundaries for different joint angle constraints.

$$L_{\max} = 2S + C \tag{17}$$

The effect of the link travel on the workspace volume is shown in Fig. 13, where $C = 1.5$ was assumed. The workspace volume approximately increases with the cubic power of the stroke.

4.2.3. Link interference. Simulation results show that link interference does not usually effect the workspace of the platform since other constraints are violated first.

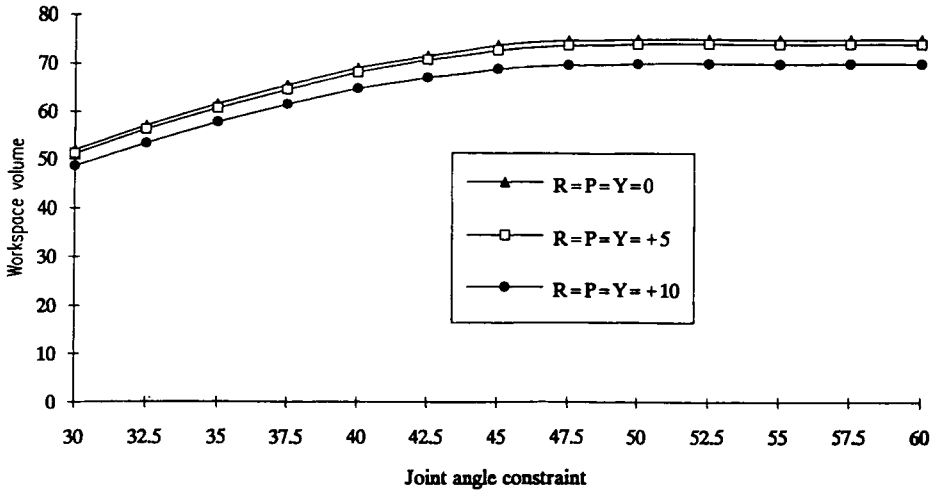

Figure 11. Workspace volume of the modified platform versus joints angle constraint.

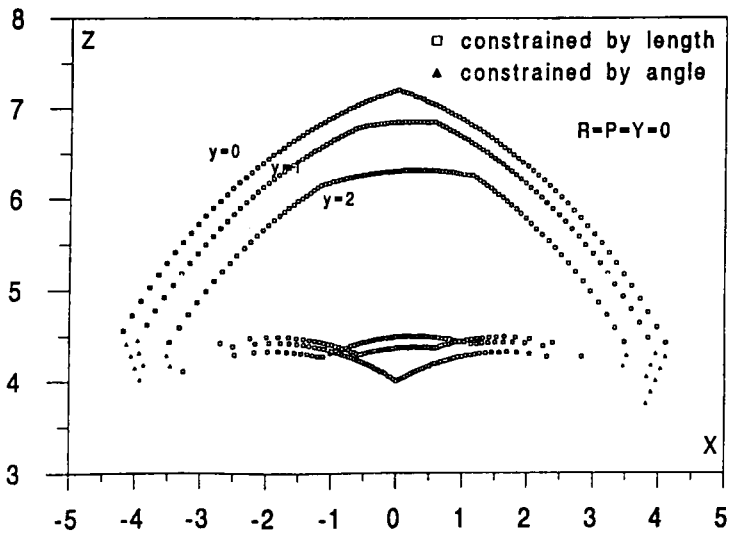

Figure 12. Workspace boundaries of the modified platform.

However, an example in which the normalized platform is rotated about the Z-axis at a constant position defined by $X = 0$, $Y = 0$ and $Z = 5$ will be used to demonstrate interference. Figure 14 illustrates the values of $\min(D_i)$, $\max(L_i)$ and $\max(\theta_b, \theta_p)$, for this special case, as a function of the rotation angle. As shown, for $D = 0.1$, link interference occurs at a roll angle of 165°. At this pose the maximum link length is about 6.4 and maximum joint angle is about 40° which means that none of these constraints were violated. However, one has to realize that this is an extreme case, and in most cases where the platform is also translated, other constraints are likely to be violated first.

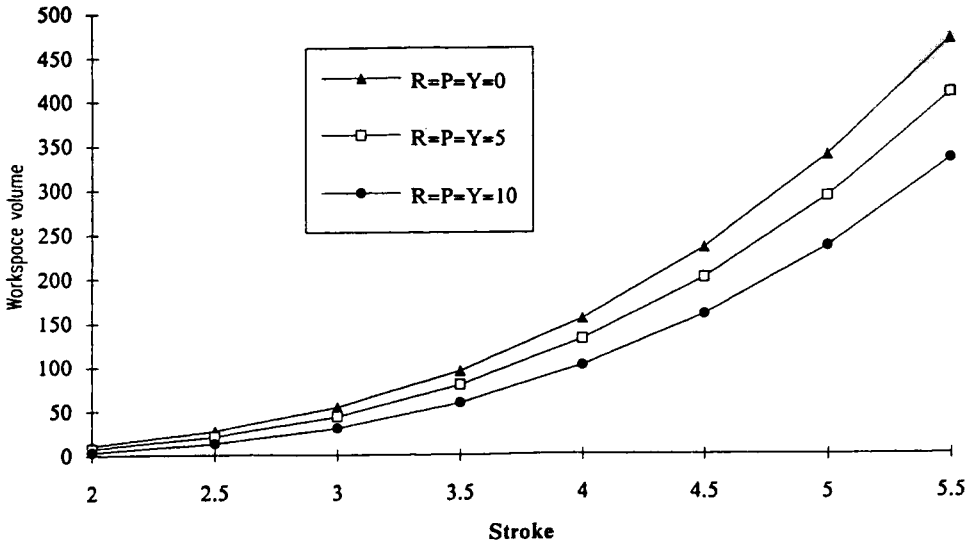

Figure 13. Workspace volume versus stroke.

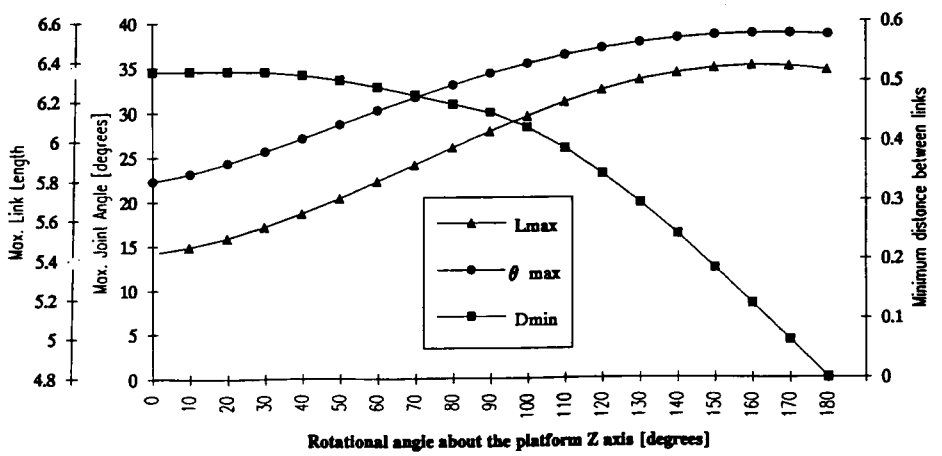

Figure 14. Platform constraints versus roll angle.

4.3. Geometric parameters

4.3.1. Joint locations. The results, shown in Fig. 15, were obtained by fixing the location of the joints on the base, defined by $R_b = 3$ and $\alpha_b = 30°$, while changing the location of the joints on the platform. It appears that the locations of the joints have little effect on the workspace. Although the maximum workspace volume is obtained at $\alpha_b = \alpha_p$, this configuration is not recommended since in such a case the Jacobian of the platform is singular [2].

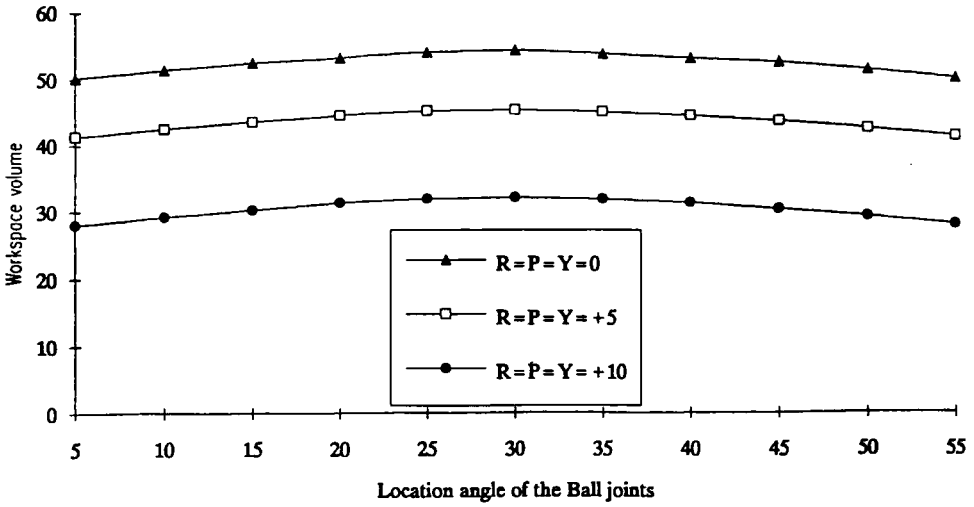

Figure 15. Workspace volume versus joints' location.

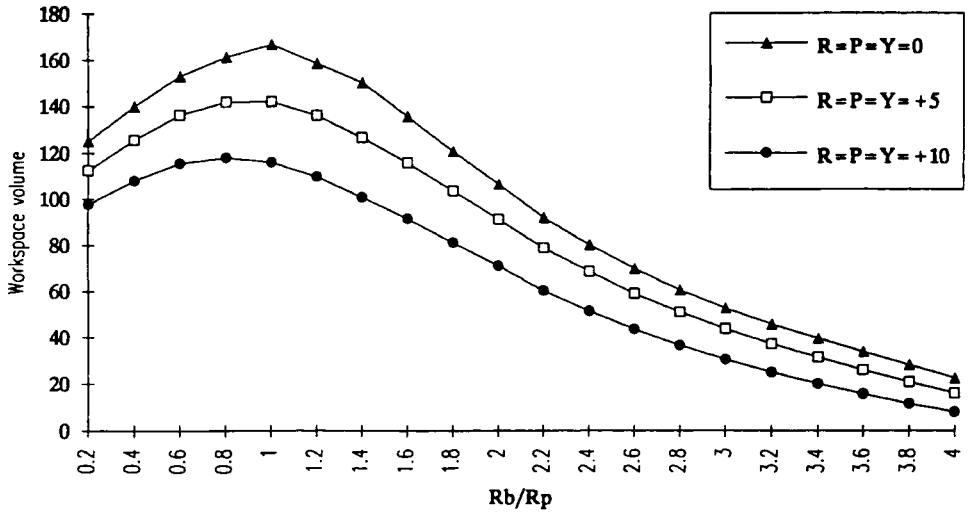

Figure 16. Workspace volume versus plate-base radii ratio.

4.3.2. Base and plate dimensions. Figure 16 shows how the platform workspace varies as a function of the ratio R_b/R_p. As shown, the volume, V, reaches it maximum value at about $R_b/R_p = 1$. For $R_b/R_p > 1.0$ the volume is constrained by link length and/or joint angle. For $R_b/R_p < 1$ the volume might be also constrained by link interference. In this particular case the platform will be locked ($V = 0$) when R_b/R_p is close to 0.1.

5. CONCLUSIONS

The analysis of the workspace volume and the dexterity of a Stewart platform, considering all kinematic constraints and platform dimensions, was presented. The workspace volumes and boundaries for different geometric parameters and kinematic constraints are computed and presented by normalized dimensions. Therefore, the information provided can be used for the selection of dimensions, joints and actuators.

REFERENCES

1. D. Stewart, "A platform with six degree of freedom," *Proc. Inst. Mech. Eng.*, vol. 180, no. 15, pp. 371–386, 1965–66.
2. E.F. Fichter, "A Stewart platform-based manipulator: general theory and practical consideration," *J. Robotic Res.*, vol. 5, no. 2, pp. 157–182, 1986.
3. K.H. Waldron and K.H. Hunt, "Series-parallel dualities in actively coordinated mechanisms," in *Proc. 4th Int. Symp. Robotics Research*, R.C. Bolles and B. Both, eds, Cambridge, MA: MIT Press, 1987, pp. 175–180.
4. K.H. Hunt, "Structural kinematic of in-parallel-actuated robot-arms," *ASME J. Mechanisms, Transmissions, and Automat. Des.*, vol. 105, pp. 705–711, 1983.
5. P. Nanua, K.J. Waldron and V. Murthy, "Direct kinematic solution of a Stewart platform," *IEEE Trans. Robotics Automat.*, vol. 6, no. 4, pp. 438–443, 1990.
6. M.Z. Huang, "On the kinematics of parallel-chain platform manipulator," in *Proc. 4th Ann. Conf. on Recent Advances in Robotics*, Boca Raton, FL, 1991, pp. 251–256.
7. J. Lee *et al.*, "Computer simulation of a parallel link manipulator," *J. Robotics Comp. Integrated Manufact.*, vol. 5, no. 4, pp. 333–342, 1989.
8. K. Sugimoto, "Kinematics and dynamics analysis of parallel manipulators by means of motor algebra," *ASME J. Mechanisms, Transmissions, and Automat. Des.*, vol. 109, pp. 3–7, 1987.
9. D.C.H. Yang and T.W. Lea, "Feasibility study of a platform type of robot manipulators from a kinematic viewpoint," *ASME J. Mechanisms, Transmissions, and Automat. Des.*, vol. 106, pp. 191–198, 1984.
10. K.M. Lee and D.K. Shah, "Kinematic analysis of a three-degree-of-freedom in-parallel actuated manipulator," *IEEE J. Robotics Automat.*, vol. 14, no. 3, pp. 354–360, 1988.
11. C.C. Nguyen and F.J. Pooran, *Kinematic Analysis and Workspace Determination of a 6 DOF CKCM Robot End-effector*. Amsterdam: Elsevier, 1989.
12. C. Gosselin, "Determination of the workspace of 6-DOF parallel manipulators," *ASME J. Mech. Des.*, vol. 112, pp. 331–336, 1990.
13. H. Zhuang and Z. Roth, "A method for kinematic calibration of Stewart platforms," in *Proc. ASME Annual Winter Meeting*, Atlanta, GA, 1991, pp. 43–48.
14. R. Hoffman and M.C. Hoffman, "Vibration models of an aircraft simulation motion systems," in *Proc. 5th World Congress for the Theory of Machines and Mechanisms*, 1979, pp. 603–606.
15. W.M. Benett, Mechanical wrist for a robot arm. BS Thesis, Mechanical Engineering, MIT, 1968.
16. H. McCallion and P.D. Truong, "The analysis of a six degree of freedom work station for mechanized assembly," in *Proc. 5th World Congress for the Theory of Machines and Mechanisms*, 1979, pp. 603–606.
17. H. McCallion, G.R. Johnson and D.T. Phan, "A compliance device for inserting a peg into a hole," *The Industrial Robot*, June, 1979.
18. W.K. Durfee, H.R. Idris and S. Dubowsky, "Real-time control of the vehicle emulation system," in *Proc. ACC Conf.*, Boston, MA, 1991, pp. 2057–2058.
19. E.F. Fichter and E.D. McDowell, "A novel design for a robot arm," in *Proc. Int. Computer Tech. Conf.*, San Francisco, CA, 1980, pp. 250–256.
20. I.L. Powell, "The kinematic analysis and simulation of the parallel topology manipulator," *Marconi Rev.*, vol. XLV, no. 226, pp. 121–128, 1982.

21. S.E. Landsburger and T.B. Sheridan, "A new design for parallel link manipulators," in *IEEE Proc. System Man and Cybernetics Conf.*, Tuscon, AZ, 1985, pp. 812–814.
22. T.B. Sheridan, "Human supervisory control of robot systems," in *Proc. Int. Conf. on Robotics and Automation*, San Francisco, CA, 1986, pp. 802–812.
23. N.G. Dagalakis, J.S. Albus, B.L. Wang and J.D. Lee, "Stiffness study of a parallel link robot crane for shipbuilding applications," in *Proc. 7th Int. Conf. on Offshore Mechanics and Arctic Engineering*, Houston, TX, 1988, pp. 29–37.
24. E.F. Fichter and E.D. MacDowell, "A novel design of a robot arm," in *ASME Int. Computer Technology Conf.*, San Francisco, CA, 1980, pp. 250–256.
25. T. Arai, K. Clearly and H. Adachi, "Design, analysis and construction of a prototype parallel link manipulator," in *Proc. IROS '90*, Tsuchiura, Ibaraki, Japan, 1990.
26. T. Arai, K. Clearly and H. Adachi, "Development of parallel link manipulator for underground excavation task," in *Proc. '91 ISART*, Tokyo, Japan, 1991.

APPENDIX A: DERIVATION OF EQUATIONS (10) AND (11)

Assume the link vectors $l_i = {}^{B}p_i - b_i$, $l_{i+1} = {}^{B}p_{i+1} - b_{i+1}$ where n_i is their common normal. The points c_i and c_{i+1} are the intersection points of n_i with l_i and l_{i+1}, respectively. As shown in Fig. A1, S_1 is a plane determined by n_i and l_{i+1} and its normal vector m_i is given by the cross-product of n_i by l_{i+1} as given in equation (11):

$$m_i = n_i \times \left({}^{B}p_{i+1} - b_{i+1}\right) \tag{A1}$$

Let the plane S_2 be parallel to S_1 and the point ${}^{B}p_i$ on plane S_2. The distance from the point b_i to S_1, $|d - b_i|$, and the distance from b_i to S_2, $|e - b_i|$, are given by:

$$\left|(b_{i+1} - b_i) \cdot m_i\right| \tag{A2}$$

and

$$\left|\left({}^{B}p_i - b_i\right) \cdot m_i\right|. \tag{A3}$$

Since the triangles $b_i {}^{B}p_i e$ and $b_i c_i d$ are similar, equation (10) is valid.

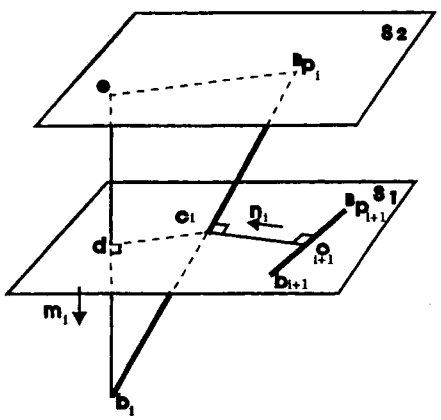

Figure A1.

ABOUT THE AUTHORS

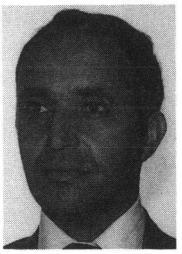

Oren Masory is a Professor of Mechanical Engineering at Florida Atlantic University in Boca Raton, Florida. He earned his BSME, MSME and PhD in 1974, 1977 and 1980, respectively, from Technion, Israel Institute of Technology, Haifa, Israel. His research interests include computer control of manufacturing systems, robotics, and application of neural networks for process monitoring and automation.

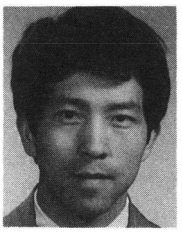

Jian Wang obtained his MS degree at the Tongji University in China (1987) and his PhD at Florida Atlantic University in USA (1992) both in Electrical Engineering. He is currently employed by Motorola Manufacturing Systems at Florida. His research interests include robot calibration and control, machine vision, and automation.